

INVESTIGATION OF STRUCTURAL, MAGNETIC AND OPTICAL PROPERTIES FOR DYSPROSIUM DOPED ZINC NANOFERRITES BY SOL-GEL AUTOCOMBUSTION TECHNIQUES

Sanchita V. Chavan^a, Vyankati R. Jadhav^a, Sunanda H. Pisal^b, Ramesh B. Bhise^{c*},
 Mahendra S. Shinde^{d*}, Vishal H. Goswami^e, Pradip B. Sarawade^f

^aPG Department of Physics, PDEA's Annasaheb Magar College, Hadpsar, Pune-28, MS, India

^bPG Department of Physics, RSS's S. M. Joshi College, Hadpsar, Pune-28, MS, India

^cPG Department of Physics, Balasaheb Jadhav Arts, Commerce and Science College, Ale (Junnar), Pune-412411, MS, India

^dDepartment of Physics, M.J.M. Arts, Commerce and Science College, Karanjali (Peth) Nashik-422208, MS, India

^eDepartment of Physics, Chikitsak Samuha's Sir Sitaram and Lady Shantabai Patkar College of Arts & Science and V.P. Varde College of Commerce & Economics, Goregaon West, Mumbai, Maharashtra 400061, India

^fDepartment of Physics, University of Mumbai, Kalina, Mumbai, India

*Corresponding Authors' e-mail: bhiseramesh@gmail.com, mahen3569@rediffmail.com

Received March 9, 2024; revised April 2, 2024; accepted April 18, 2024

Using the auto combustion sol-gel method, nanoferrite crystalline aligns of Dy³⁺ replaced Zn-Fe spinel ferrite with the chemical formula Dy_xZn_{1-x}Fe_{2-x}O₄ (x= 0.00, 0.05) were successfully synthesized. In this process, citric acid was utilized as energy (fuel) in a 3:1 ratio to metal nitrate. Using XRD and FT-IR, the crystal structure and phase of dysprosium zinc was examined. Using the XRD method, the crystal size, lattice constant, cation distribution, and porosity were ascertained. FT-IR spectroscopy is used to infer structural study and the redistribution of cations between octahedral (A) and tetrahedral (B) site of Zn material. According to morphological research, the temperature during sintering is what causes grain to form and grow. Utilizing the Hysteresis Loop Technique, saturation magnetism and magneton number are determined. In Zn-Fe ferrite, the saturation magnetization rises with increasing density x, utilizing the Sol-gel auto-combustion method at a comparatively low temperature. Using nitrate citrate, the nanocrystallite Dy_xZn_{1-x}Fe_{2-x}O₄ was created. The combustion process and chemical gelation are unique. Using citric acid as a catalyst, their metal nitrates nanoferrites underwent a successful chemical reaction and were obtained as a dried gel. FT-IR, UV-Visible, VSM and XRD were used to characterize the produced nanoferrite powders. Magnetization and hysteresis were measured using the VSM technique. The FT-IR verifies that the synthesized substance is ferrite. The size of the nanocrystalline ferrite material, Dy_xZn_{1-x}Fe_{2-x}O₄, was determined by X-ray using the Scherrer method to be between 16.86 to 12.72 nm average crystallite size. Magnetization and hysteresis were measured using the VSM technique.

Keywords: Autocombustion technique; VSM technique; FT-IR spectroscopy; UV-Visible Spectroscopy; XRD method

PACS: 75.50.Gg, 75.75.+a, 76.60.Es

1. INTRODUCTION

Substituted rare earth materials with different ferrites are emerging as promising materials with a range of uses. Depending on the kind and quantity of rare earth element utilized, the addition of a small amount of rare earth to iron oxide samples changes their electrical, magnetic, and structural properties. Two categories exist for rare earth ions: one has a radius that is similar to that of iron ions, while the other has a radius that is larger [1]. This variation in ionic radii will cause micro strain, which could cause the spine's structure to deform [2]. Because of their large ionic radii, rare earth ions replaced Fe³⁺ in the ferritin mixture, resulting in limited soluble in the spinel lattice [3]. It is discovered that the rare earth ions are a promising addition to enhance ferrites' magnetic characteristics [4-5]. Sm³⁺ doped Cu-Zn ferrite [6] and La³⁺ doped Ni-Cu-Zn ferrite [5] are two examples of rare earth doped ferrites.

Researchers used a variety of techniques to create zinc ferrite nanoparticles, such as hydrothermal, solgel auto-combustion, combination, sonochemical, the microemulsion, reverse micelle, and high energy ball milling [7-10]. Due to its low cost, heat at low temperatures treatment, and ease of handling in comparison to other methods, sol-gel autocombustion is one of the most widely used methods for preparing nano-scale ferrite powder [11]. The physical properties of zinc ferrite nanoparticles are influenced by grain size and cation distribution at A- and B-sites in the spinel ferrite lattice. Doping spinel ferrite nanoparticles with different rare earth ions in small amounts has recently emerged as a promising strategy for improving their physical properties [12].

In the current study, dysprosium-doped Zinc ferrite was synthesized using the sol-gel auto combustion method [13]. The following techniques were used to characterize these ferrite materials: electrical resistivity, magnetic hysteresis, TGA-DTA, XRD, FT-IR. This dysprosium doped Zn ferrite material's catalytic activity was investigated for the breakdown of hydrogen peroxide. It had demonstrated that the rate constant increases as the amount of Dy in ZnFe₂O₄ [x=0.0, 0.050] increases.

2. MATERIALS AND METHODS

2.1 Materials

Chemicals of reagent grade purity were used. We prepared solutions of zinc nitrate, iron nitrate, dysprosium nitrate, and ammonia in deionized water. The added to a beaker containing 0.25 M zinc nitrate solution. Added to it after that were solutions of dysprosium nitrate and 0.25 M iron nitrate. This mixture was mixed with citric acid solution, and ammonia solution was added while stirring continuously to bring the pH to 7. To create gel, this mixture was agitated and heated to 80°C for three hours. To get Dy-Zn ferrite powder, this gel was heated on a hot plate between 300°C. This powder was used for characterization after being calcined for 4-5 hours at 500 °C.

2.2 Characterization techniques

The structural characterization and phase identification were examined using X-Ray Diffraction (XRD), (Rigaku miniflex 600), fitted with a high-intensity Cu-k radiation source ($\lambda = 1.5406$) in the 2θ range ($20^\circ-80^\circ$) with a step size of 0.0260 at room temperature. FTIR (Thermo Nicolet, Avatar 370) recorded the room temperature Fourier transform infrared spectra in the wavenumber range of 4000-400 cm^{-1} . A Vibrating Sample Magnetometer (VSM) with a maximum applied magnetic field range was used to measure the magnetic characteristics of the sample at room temperature.

3. RESULT AND DISCUSSION

3.1 XRD Analysis

The X-ray diffraction structure for $\text{ZnDy}_x\text{Fe}_{2-x}\text{O}_4$ ($x=0.00, 0.05$) spinel ferrite nano particles that were synthesized using the sol-gel method. The samples of Zn composites were sintered for five hours at 500 °C. The XRD was used to determine the structure of the crystal and crystalline phase pattern. This is an extremely useful method for calculating crystalline parameters.

Fig. 1(a). The diffraction peaks observed in the XRD pattern of prepared samples corresponded to the crystal planes (311), (400), (332), (530), (631) and (643) respectively. The presence of all diffraction peaks of nanoparticles that have been synthesized makes certain the formation of the cubic inverse spinel structure, the sign denotes the mixed impurity phase of DyFeO_3 . Because of its larger ionic radius, the substitution of Fe^{3+} ions by Dy^{3+} ions have a solubility limit. As a result, the amount of Fe^{3+} ions that can be replaced by Dy^{3+} ions are limited. Because of its larger ionic radius, the substitution of Fe^{3+} ions by Dy^{3+} ions have a solubility limit. As a result, the amount of Fe^{3+} ions that will be replaced by Dy^{3+} ions are limited. As a result of an excess substitute of Dy^{3+} ions, it is expected that DyFeO_3 phase will develop together the grain boundaries, as observed [14].

The crystallite sizes were determined using equations 1 are shown in Table 1, and the W-H plots $\beta\cos\theta$ versus $4\sin\theta$ for samples that were synthesized are shown in Fig. 1(b). The intercept used to determine the crystal size (D) was calculated was provided by a linear plot, and the strain value was computed by a straight line fitting of the slope. The crystallite sizes of $\text{Zn Dy}_x\text{Fe}_{2-x}\text{O}_4$ are smaller than those of pure zinc ferrite due to differences in the ionic radii of doped ions and substituted ions from the interstitial sites, and the results are consistent with ref. [15,16,17].

Figure 1 depicts an XRD pattern. The average size of the crystallite (Dm) was calculated using the Debye Scherrer formula, which is given as:

$$D = k\lambda/\beta\cos\theta \quad (1)$$

Where, k is 0.9 for spinel ferrites; λ is the 1.54 indicates the x-ray wavelength; β is the FWHM of the most intense peak, and is the diffraction angle of the most intense peak.

The average lattice parameter 'a' can be calculated using the formula:

$$a = \sqrt{h^2 + k^2 + l^2} \quad (2)$$

Where, d is the crystal plane spacing; hkl is the miller index value

The average lattice constant for all samples was found to be in the range of 8.44 to 8.33. The ionic radiuses. The average lattice parameter 'a' was explained using the ions Dy^{3+} and Fe^{3+} . The average lattice parameter was found to decrease as the Dy^{3+} doping content increased. The following formula can be used to calculate X-ray density ρ_x :

$$\rho_x = \frac{8M}{Na^3}, \quad (3)$$

where,

M is the molecular weight of the composition Z=8 for spinel structure represents the number of molecules per unit cell, N is the Avogadro number (6.0221×10^{23}), and a^3 is the volume of the unit cell.

The X-ray density was calculated to be between 7.48 and 21.23 g/cm^3 . Because Dy^{3+} has a higher molar weight than Fe^{3+} , the relationship between X-ray density and quantity is almost linear [12]. This means that the X-ray density increases as the amount of Dy^{3+} doping increases.

The Micro-strain calculated by using this formula

$$\text{Micro-strain} = \frac{\beta\cos\theta}{4} (10^{15}) \quad (4)$$

Micro-strain was calculated to be between 0,0021 and 0.0029. As the concentration of Dy³⁺ doping increases, the micro-strain decreases. At x = 0.00, 0.05 the highest value of micro-strain was observed. The dislocation density of the nanoparticles that can be calculated using the following equation:

$$\delta = \frac{1}{D^2}(10^{15}) \tag{5}$$

Where, D is the crystalline size.

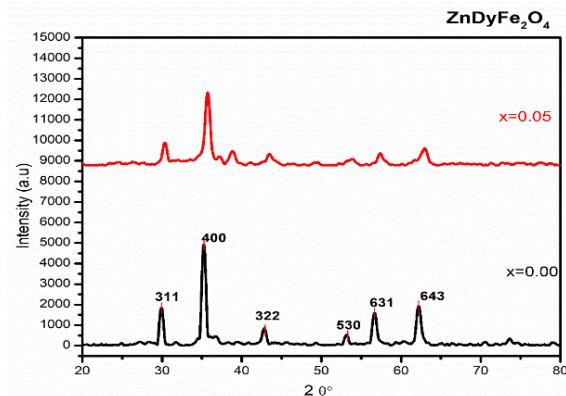


Figure 1(a). XRD Analysis of Dy³⁺ Zn ferrite (x=0.00,0.05)

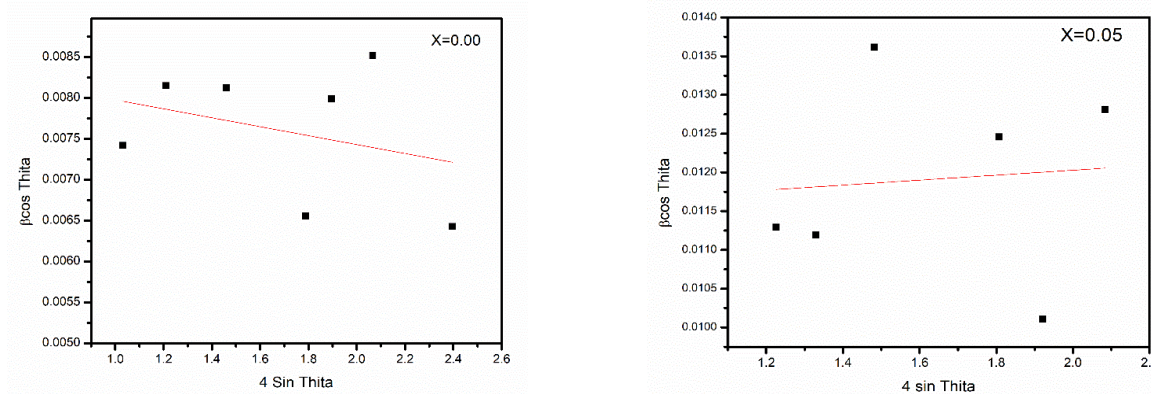


Figure 1(b). Hall – Williamson plots of ZnDyFe₂O₄ (x=0.00, 0.05)

Table 1. Measurement of Lattice Constat, Density and Micro-strain, etc.

Content x	Interplanar distance	Lattice parameter (Å°)	X ray Density	Crystalline size (nm)	Micro-strain	Dislocation Density (×10 ¹⁴) line/m ²
0.00	2.5465	8.4469	4.2597	17.77	0.0021	0.0084
0.05	2.5120	8.3323	4.4378	12.83	0.0029	0.0237

3.2 FT-IR Analysis

As shown in Fig. 2, the FT-IR spectra of the ZnDy_xFe_{2-x}O₄ samples are obtained in the 4000 to 500 cm⁻¹ range.

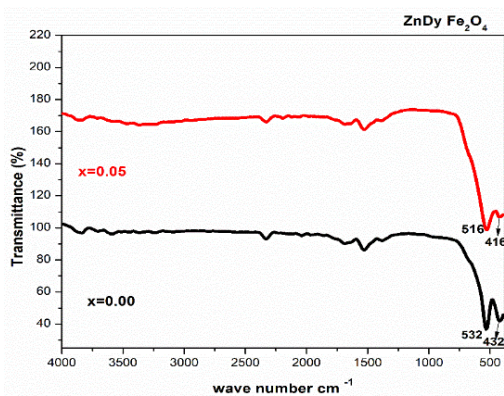


Figure 2. FT-IR spectra of Dy³⁺ doped Zn ferrite (x=0.00,0.05)

Ferrite exhibits two prominent oxygen-metal frequencies [18]. The tetrahedral (A) and octahedral (B) metal stretching, which are thought to be the typical bands of spinel structure, were associated with the higher frequency band (ν_1) and lower frequency band (ν_2) which were observed in the range of 532-516 cm^{-1} and 432-416 cm^{-1} [19].

The absorption frequency values, ν_1 and ν_2 that as the Dy^{3+} content increased, the absorption frequency ν_2 was slightly moved towards a higher frequency and ν_1 towards a lower frequency side. This is explained by the Fe^{3+} ions on the tetrahedral site shifting in the direction of the oxygen ions, which reduces with the $\text{Fe}^{3+}\text{-O}^2$ distance. The basic frequency and central frequency decrease as the site radius increases, which changes to the underside Literature has documented similar reports [20-21].

3.3 VSM Analysis

For VSM analysis Figure 3 shows Hysteresis loop of Zn Dy^{3+} -doped Zn ferrite ($x=0.00, 0.05$). The Saturation Magnetization (M_s), Coercivity (H_c), and Remnant ratio ($R=Mr/M_s$) of each sample are listed in Table 2. The values of M_s and M_r for pure zinc ferrite have decreased from 1248.0914 to 041.0400 emu/g and 301.2114 to 301.2114 emu/g, respectively, while the coercivity has increased from 058.8889 to 050.5556 Oe. The decrease in M_s with Dy content is in line with the findings of ferrites doped with rare earth elements [22]. Tables show that there is a direct correlation between the size of the nanoferrite particles and the value of M_s [23].

Table 2 shows that when Dy^{3+} is substituted, the magnetization values decrease. The site use of the cations and the changes in the exchange effects brought about by the adding of dysprosium can be used to explain the trend. The primary source of magnetic properties is Fe^{3+} on the cubic spinal B-sites. Due to its strong octahedral preference, the dysprosium ion takes up residence at the B-site, causing the Fe^{3+} ion to migrate to the A-site.

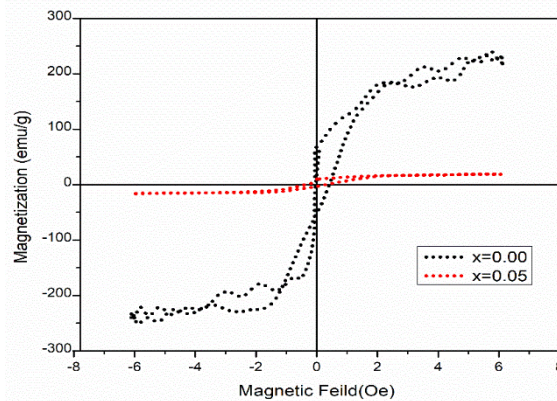


Figure 3. Hysteresis loop of Zn Dy^{3+} -doped Zn ferrite ($x=0.00, 0.05$)

Table 2. Measurement of Saturation Magnetization (M_s), Coercivity (H_c), and Remnant ratio

Composition (x)	H_c (Oe)	M_r (emu/gm)	M_s (emu/gm)
0.00	050.5556	301.2114	1248.0914
0.05	058.8889	301.2114	041.0400

3.4 UV-Visible analysis

The Diffuse Reflectance Spectroscopy (DRS) optical absorption spectra in the absorption mode for $\text{ZnDyFe}_2\text{O}_4$ nanoparticles (where $x = 0.00, 0.05$) within the UV-visible range are shown in Figure 4.

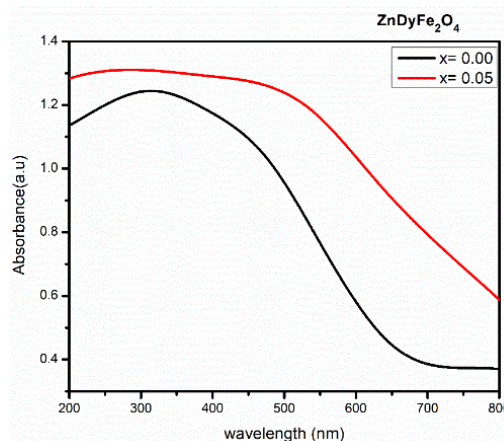


Figure 4. Absorbance spectra of $\text{ZnDyFe}_2\text{O}_4$ system ($x=0.00, 0.05$)

These samples were prepared at room temperature and sintered at 500°C. Three absorption bands are observed at 416 nm and 518 nm, which is in line with the XRD findings. The composition and heat treatment of the samples influence the nature of this absorption, as shown in Figure 4. Three different types of electronic transitions are seen in the optical absorption of ZnDyFe₂O₄ samples. Specifically, for the x = 0 composition sample, electronic transitions related to charge carriers are observed in the wavelength range of 200 to 800 nm within the optical region.

The calculated band gap energy decreases from 2.9807 to 2.3938 eV for samples sintered at 500°C [24].

$$\text{Energy band gap} = 1240/\pi(\text{nm}) \quad (6)$$

4. CONCLUSION

Spinel ferrites nanoparticles have an important role in our daily lives and are used in a variety of applications including medical sectors, nano electronics, and the treatment of waste water, among others. Dysprosium (Dy³⁺) substituted Zn nanoferrites with the general formula ZnDy_xFe_{2-x}O₄ (x = 0.00, 0.05) were successfully synthesized using the sol-gel autocombustion method, which is the simplest method for producing such nano ferrites. The decrease in average crystalline size from 16.86 to 12.72 nm is the result of Dy³⁺ substitution on the structural characteristics of zinc ferrite.

FT-IR was used to confirm the spinel phase structure. The characteristics of spinel structure are divided into two primary frequency bands: the higher frequency band ν_1 (approx. 532 cm⁻¹) and the lower frequency band ν_2 (approx. 432 cm⁻¹). The absorption peaks are referred to as higher frequency bands ν_1 due to the tetrahedral site of inherent increasing vibration. Lower frequency bands ν_2 are referred to as octahedral stretching bands.

ORCID

✉ Mahendra S. Shinde, <https://orcid.org/0000-0001-9141-5049>; ✉ Vishal H. Goswami, <https://orcid.org/0000-0001-9782-2737>

REFERENCES

- [1] N. Rezlescu, E.C. Rezlescu, and M.L. Craus, "Effects of the rare-earth ions on some properties of a nickel-zinc ferrite," *J. Phys. Condens. Matter.* **6**, 5707 (1994). <https://doi.org/10.1088/0953-8984/6/29/013>
- [2] S. Solyman, "Transport properties of La-doped Mn-Zn ferrite," *Ceram. Int.* **32**, 755-760 (2006). <https://doi.org/10.1016/j.ceramint.2005.05.018>
- [3] A.A. Sattar, and K.M. El-Shokrofy, "Rare Earth Doping Effect on the Electrical Properties of Cu-Zn Ferrites," *J. Phys.* **7**(1), C1-245-C1-246 (1997). <https://doi.org/10.1051/jp4:1997194>
- [4] N. Rezlescu, E. Rezlescu, P.D. Mangeron, L. Rezlescu, and C. Pasnicu, "The Influence of R₂O₃ (R = Yb, Er, Dy, Tb, Gd, Sm and Ce) on the Electric and Mechanical Properties of a Nickel-Zinc Ferrite," *J. Phys. C: State Solid*, **162**, 673-678 (1997). [https://doi.org/10.1002/1521-396X\(199708\)162:2%3C673::AID-PSSA673%3E3.0.CO;2-A](https://doi.org/10.1002/1521-396X(199708)162:2%3C673::AID-PSSA673%3E3.0.CO;2-A)
- [5] P.K. Roy, B.B. Nayak, and J. Bera, "Study on electro-magnetic properties of La substituted Ni-Cu-Zn ferrite synthesized by auto-combustion method," *J. Magn. Magn. Mater.* **320**, 1128-1132 (2008). <https://doi.org/10.1016/j.jmmm.2007.10.025>
- [6] A.A. Sattar, A.H. Wafik, K.M. El-Shokrofy, and M.M. El-Tabby, "Magnetic Properties of Cu-Zn Ferrites Doped with Rare Earth Oxides," *Status Solidi a*, **171**, 563-569 (1999). [https://doi.org/10.1002/\(SICI\)1521-396X\(199902\)171:2%3C563::AID-PSSA563%3E3.0.CO;2-K](https://doi.org/10.1002/(SICI)1521-396X(199902)171:2%3C563::AID-PSSA563%3E3.0.CO;2-K)
- [7] B. Azhdar, B. Stenberg, and L. Kari, "Polymer-nanofiller prepared by high-energy ball milling and high velocity cold compaction," *Polymer Composites*, **29**, 252-261 (2008). <https://doi.org/10.1002/pc.20353>
- [8] N. Javerberg, H. Edin, P. Nordell, S. Nawaz, B. Azhdar, and U.W. Gedde, "Dielectric properties of alumina-filled poly (ethylene-co-butyl acrylate) nanocomposites. Part I-dry studies," *IEEE Trans. Dielectr. Electr. Insul.* **19**(2), 383-390 (2012). <https://doi.org/10.1109/TDEI.2012.6180229>
- [9] J. Peng, M. Hojamberdiev, Y. Xu, B. Cao, J. Wang, and H. Wu, "Hydrothermal synthesis and magnetic properties of gadolinium-doped CoFe₂O₄ nanoparticles," *J. Magn. Magn. Mater.* **323**(1), 133-137 (2011). <https://doi.org/10.1016/j.jmmm.2010.08.048>
- [10] M.A. Almessiere, Y. Slimani, S. Guner, M. Sertkol, A. Demir Korkmaz, S.E. Shirsath, and A. Baykal, "Sonochemical synthesis and physical properties of Co_{0.3}Ni_{0.5}Mn_{0.2}Eu_xFe_{2-x}O₄ nano-spinel ferrites," *Ultrasonics Sonochemistry*, **58**, 104654 (2019). <https://doi.org/10.1016/j.ultsonch.2019.104654>
- [11] V.S. Rizi, F. Sharifianjazi, H. Jafarikhorami, N. Parvin, L.S. Fard, M. Irani, and A. Esmailkhanian, "Sol-gel derived SnO₂/Ag₂O ceramic nanocomposite for H₂ gas sensing applications," *Materials Research Express*, **6**, 1150g-1152g (2019); <https://doi.org/10.1088/2053-1591/ab511e>
- [12] R.S. Yadav, I. Kuřitka, J. Vilcakova, J. Havlica, L. Kalina, P. Urbánek, M. Machovsky, et al., "Sonochemical synthesis of Gd³⁺ doped CoFe₂O₄ spinel ferrite nanoparticles and its physical properties," *Ultrason. Sonochem.* **40**, 773-783 (2018). <https://doi.org/10.1016/j.ultsonch.2017.08.024>
- [13] P. Ravindranathan, and K.C. Patil, "A low temperature path to the preparation of ultrafine ferrites," *Ceram. Bull.* **66**, 688-692 (1987). <http://eprints.iisc.ac.in/id/eprint/13867>
- [14] I.K. Punithavathy, A. Rajeshwari, S.J. Jeyakumar, N. Lenin, B. Vigneshwaran, M. Jothibas, and B. Arunkumar, "Impact of lanthanum ions on magnetic and dielectric properties of Zinc nanoferrites," *J. Mater. Sci. Mater. Electron.* **31**, 9783-9795 (2020). <https://doi.org/10.1007/s10854-020-03523-3>
- [15] K.L. Routray, S. Saha, and D. Behera, "Rare-earth (La³⁺) substitution induced changes in the structural, dielectric and magnetic properties of nano- CoFe₂O₄ for highfrequencyand magneto-recording devices," *Appl. Phys. A*, **125**, 328 (2019). <https://doi.org/10.1007/s00339-019-2615-8>
- [16] S.B. Das, R.K. Singh, V. Kumar, N. Kumar, P. Singh, and N.K. Naik, "Structural, magnetic, optical and ferroelectric properties of Y³⁺ substituted zinc ferrite nanomaterials prepared by a cost-effective sol-gel route," *Mater. Sci. Semicond. Process.* **145**, 106632 (2022). <https://doi.org/10.1016/j.mssp.2022.106632>

- [17] S.S. Satpute, S.R. Wadgane, K. Desai, D.R. Msne, and R.H. Kadam, "Substitution effect of Y^{+3} ions on the structural, magnetic and electrical properties of zinc ferrite nanoparticles," *Ceramica*, **66**, 43–49 (2020). <https://doi.org/10.1590/0366-69132020663772734>
- [18] K.V. Kumar, "Tunable optical bandgap of gadolinium substituted nickel-zinc ferrite nanoparticles-effect of calcination temperature on its optical parameters," *Advances in Materials Physics and Chemistry*, **12**, 33–45 (2022). <https://doi.org/10.4236/ampc.2022.123003>
- [19] M. Rashad, R. Mohamed, and H. El-Shall, "Magnetic properties of nanocrystalline Sm-substituted $CoFe_2O_4$ synthesized by citrate precursor method," *J. Mater. Process. Technol.* **198**, 139-146 (2008). <https://doi.org/10.1016/j.jmatprotec.2007.07.012>
- [20] F.-X. Cheng, J.-T. Jia, Z.-G. Xu, B. Zhou, C.-S. Liao, C.-H. Yan, L.-Y. Chen, and H.- B. Zhao, "Microstructure, magnetic, and magneto-optical properties of chemical synthesized Co-RE ($RE=Ho, Er, Tm, Yb, Lu$) ferrite nanocrystalline films," *J. Appl. Phys.* **86**, 2727-2732 (1999). <https://doi.org/10.1063/1.371117>
- [21] A. Gadkari, T. Shinde, and P. Vasambekar, "Structural analysis of Y^{3+} -doped Mg-Cd ferrites prepared by oxalate coprecipitation method," *Mater. Chem. Phys.* **114**, 505-510 (2009). <https://doi.org/10.1016/j.matchemphys.2008.11.011>
- [22] J. Peng, M. Hojamberdiev, Y. Xu, B. Cao, J. Wang, and H. Wu, "Hydrothermal synthesis and magnetic properties of gadolinium-doped $CoFe_2O_4$ nanoparticles," *J. Magn. Magn. Mater.* **323**, 133-137 (2011). <https://doi.org/10.1016/j.jmmm.2010.08.048>
- [23] A. Goldman, *Modern Ferrite Technology*, 2nd ed. (Springer, Pittsburgh, 2006).
- [24] V. Awati, K. Badave, and D. Bobade, "Effect of Tb^{3+} substitution on structural, optical and magnetic properties of $NiCuZnFe_2O_4$ prepared by sol-gel route," *Indian J. of Physics*, **96**(1), 89–101 (2022). <https://doi.org/10.1007/s12648-020-01955-5>

ДОСЛІДЖЕННЯ СТРУКТУРНИХ, МАГНІТНИХ ТА ОПТИЧНИХ ВЛАСТИВОСТЕЙ НАНОФЕРИТІВ ЦИНКУ, ЛЕГОВАНИХ ДИСПРОЗИЄМ ШЛЯХОМ ЗОЛ-ГЕЛЬ АВТОЗГОРЯННЯ

Санчіта В. Чаван^a, В'янкати Р. Джадхав^a, Сунанда Х. Пісал^b, Рамеш Б. Бхісе^c, Махендра С. Шінде^d, Вішал Х. Госвами^e, Прадіп Б. Саравале^f

^aPG Департамент фізики, Коледж Аннасахеба Магара PDEA, Хадпсар, Пуна-28, MS, Індія

^bДепартамент фізики, Коледж С. М. Джоші RSS, Хадпсар, Пуна-28, MS, Індія

^cPG Департамент фізики, Коледж мистецтв, торгівлі та науки Баласахеба Джадхава, Але (Джуннар), Пуна, MS, Індія

^dДепартамент фізики, М.І.М. Коледж мистецтв, торгівлі та науки, Каранджалі (Пет) Нашік-422208, MS, Індія

^eДепартамент фізики, коледж мистецтв та наук сера Сітарам та леді Шантабай Паткар Чикітасак Самуха та коледж торгівлі та економіки Варде, Західний Горгаон, Мумбаї, Махараштра 400061, Індія

^fДепартамент фізики, Університет Мумбаї, Каліна, Мумбаї, Індія

Використовуючи золь-гель метод автоматичного спалювання, було успішно синтезовано кристалічні угруповання нанофериту Du^{3+} , заміненого шпінельним феритом Zn-Fe з хімічною формулою $Du_xZn_{1-x}Fe_{2-x}O_4$ ($x= 0,00, 0,05$). У цьому процесі лимонна кислота використовувалася як енергія (паливо) у співвідношенні 3:1 до нітрату металу. За допомогою XRD та FT-IR досліджено кристалічну структуру та фазу диспрозую цинку. Методом XRD встановлено розмір кристалів, постійну ґратки, розподіл катіонів і пористість. FT-IR спектроскопія використовується для висновку про структурне дослідження та перерозподіл катіонів між октадральним (А) і тетрадральним (В) матеріалом Zn. Згідно з морфологічними дослідженнями, температура під час спікання є причиною формування та росту зерна. Використовуючи методику петлі гістерезису, визначають магнетизм насичення та число магнетонів. У ферити Zn-Fe намагніченість насичення зростає зі збільшенням щільності x , з використанням методу золь-гель автоспалювання при порівняно низькій температурі. Використовуючи цитрат нітрату, створено нанокристаліт $Du_xZn_{1-x}Fe_{2-x}O_4$. Процес горіння і хімічне гелеутворення унікальні. Використовуючи лимонну кислоту як каталізатор, їхні наноферити з нітратів металів пройшли успішну хімічну реакцію та були отримані у вигляді висушеного гелю. FT-IR, UV-Visible, VSM та XRD були використані для характеристики отриманих наноферитових порошків. Намагніченість і гістерезис вимірювали за допомогою методу VSM. FT-IR підтверджує, що синтезована речовина є феритом. Розмір нанокристалічного феритового матеріалу, $Du_xZn_{1-x}Fe_{2-x}O_4$, був визначений рентгенівським методом за допомогою методу Шеррера, коли середній розмір кристалітів становить від 16,86 до 12,72 нм. Намагніченість і гістерезис вимірювали за допомогою методу VSM.

Ключові слова: техніка автозгоряння; техніка VSM; FT-IR спектроскопія; УФ-видима спектроскопія; метод XRD